Cell Reports
Methods

Report

An intravitreal implant injection method for sustained drug delivery into mouse eyes

Graphical abstract

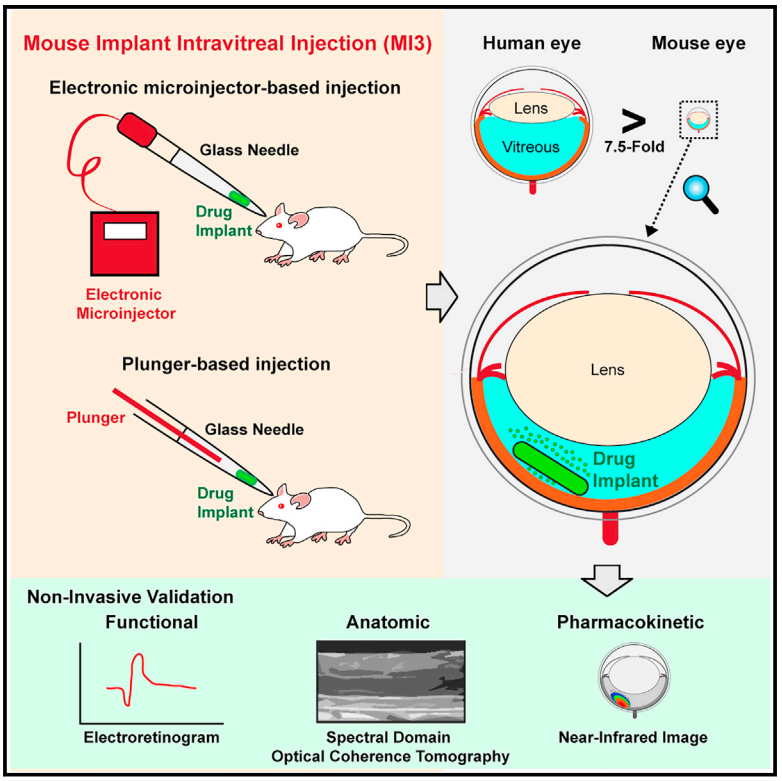

Highlights

- Surgical method for intravitreal injection of ocular drug implants into mouse eyes
- Robust tools allow functional testing in mouse genetic models of human eye disease
- Sustained release of small molecule drugs can be noninvasively monitored in mouse eyes

Authors

Young Joo Sun, Cheng-Hui Lin, Man-Ru Wu, ..., Youn Soo Jung, Sui Wang, Vinit B. Mahajan

Correspondence

vinit.mahajan@stanford.edu (V.B.M.), suiwang@stanford.edu (S.W.)

In brief

Ocular drug implants (ODIs) that slowly release small molecules into the eye are a therapeutic approach for retinal diseases. Yet a lack of ODI delivery methods in mouse disease models limits ODI development. Sun et al. present a simple, robust, and safe surgical method for ODI delivery into mouse eyes.

Sun et al., 2021, Cell Reports Methods *1*, 100125
December 20, 2021
https://doi.org/10.1016/j.crmeth.2021.100125

CellPress

Cell Reports Methods

CellPress
OPEN ACCESS

Report

An intravitreal implant injection method for sustained drug delivery into mouse eyes

Young Joo Sun,[1,5] Cheng-Hui Lin,[2,5] Man-Ru Wu,[2] Soo Hyeon Lee,[1] Jing Yang,[1] Caitlin R. Kunchur,[1] Elena M. Mujica,[1] Bryce Chiang,[2] Youn Soo Jung,[1,3] Sui Wang,[2,*] and Vinit B. Mahajan[1,4,6,*]

[1]Molecular Surgery Laboratory, Byers Eye Institute, Department of Ophthalmology, Stanford University, Palo Alto, CA 94304, USA
[2]Byers Eye Institute, Department of Ophthalmology, Stanford University, Stanford, CA 94304, USA
[3]Department of Epidemiology and Clinical Research, Stanford University School of Medicine, Stanford, CA 94305, USA
[4]Veterans Affairs Palo Alto Health Care System, Palo Alto, CA 94304, USA
[5]These authors contributed equally
[6]Lead contact
*Correspondence: vinit.mahajan@stanford.edu (V.B.M.), suiwang@stanford.edu (S.W.)
https://doi.org/10.1016/j.crmeth.2021.100125

MOTIVATION Ocular drug implants (ODIs) that slowly release therapeutic small molecules into the eye could provide significant advantages for the treatment of chronic retinal disease, both by expanding therapeutic access to new classes of medications and by avoiding the need for indefinite monthly intravitreal injections of therapeutics, such as antibodies, to treat diseases such as age-related macular degeneration and diabetic retinopathy. Genetically modified mice are commonly used to model human retinal disease. However, many therapeutic molecules are not tested in mice because their eyes are orders of magnitude smaller than human eyes and methods for ODI delivery into such small eyes are lacking. Here, we present a method to deliver an ODI into the mouse vitreous, thus expanding ODI and small molecule research and therapeutic testing in mouse models of human eye disease.

SUMMARY

Using small molecule drugs to treat eye diseases carries benefits of specificity, scalability, and transportability, but their efficacy is significantly limited by a fast intraocular clearance rate. Ocular drug implants (ODIs) present a compelling means for the slow and sustained release of small molecule drugs inside the eye. However, methods are needed to inject small molecule ODIs into animals with small eyes, such as mice, which are the primary genetic models for most human ocular diseases. Consequently, it has not been possible to fully investigate efficacy and ocular pharmacokinetics of ODIs. Here, we present a robust, cost-effective, and minimally invasive method called "mouse implant intravitreal injection" (MI3) to deliver ODIs into mouse eyes. This method will expand ODI research to cover the breadth of human eye diseases modeled in mice.

INTRODUCTION

Ocular drug implants (ODIs) are controlled release devices that can maintain ocular drug concentrations at therapeutic levels for prolonged durations. Controlled drug release over extended periods of time can greatly reduce dosing frequency, which can improve medication adherence in patients and reduce risk during procedures if the drug needs frequent intraocular injection (Parsons et al., 2021). ODIs can be especially beneficial for treating slow-progressing, chronic posterior segment eye diseases, such as age-related macular degeneration, diabetic retinopathy, and retinitis pigmentosa. As of June 2021, there are five FDA-approved ODIs (Ozurdex, Iluvien, YUTIQ, Retisert, and Triesence) to treat posterior segment eye diseases with many more in various stages of clinical and preclinical development; yet, they are all steroid formulations. Two of the most commonly used ODIs, Ozurdex and Iluvien, are treatments for diabetic macular edema and can maintain therapeutic ocular levels of dexamethasone for more than 6 months and 2–3 years, respectively.

Small molecule drugs can target disease molecules in the eye, but they have not been investigated since there is rapid clearance. Numerous genetically modified mice that model human ocular disease are used in translational studies to validate gene therapy and antibody therapies, but not small molecule drugs. An ODI formulation strategy could provide an opportunity to expand the therapeutic toolbox because there are technical, target, and safety limits to gene therapy and antibody therapies (Chames et al., 2009; Uddin et al., 2020). Currently, preclinical

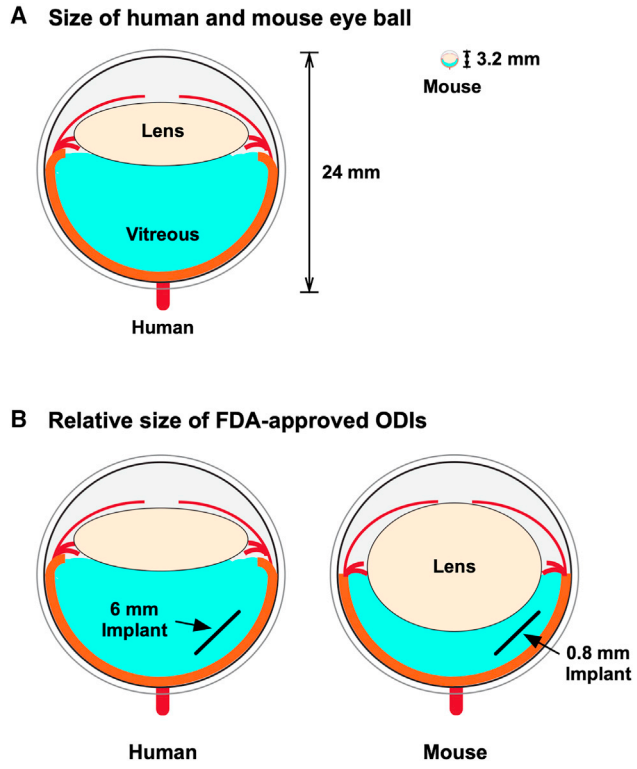

Figure 1. Mouse eyeballs are orders of magnitude smaller than human eyeballs

(A) The diameter of the human eyeball is compared to that of the mouse eyeball.

(B) Relative size of mouse ODI is shown based on FDA-approved human ODIs.

characterization of ODIs, including pharmacokinetics and toxicity, is carried out in rats, rabbits, pigs, and non-human primates because their eye size and anatomy are more similar to humans. For these mammalian models, ODIs were inserted using an incision or a specialized ODI injector for humans with a needle wider than 22 gauge (El-Ghrably et al., 2015; Haller et al., 2010; Moisseiev et al., 2014), both of which are too disruptive for small mouse eyes. Compared to mouse models, testing ODIs in larger mammalian models is expensive, time consuming, and, most importantly, limited by the small number of available ocular disease models available to test *in vivo* efficacies. Because of these limitations, a robust and less-invasive intraocular implant delivery method for animal models with small eyes is a top priority.

In humans, intravitreal injection is a simple, quick, and painless intraocular delivery method for soluble or colloidal ocular drugs widely used in both clinics and laboratories. However, the conventional intravitreal injection tools are limited for implanting solid ODIs into mouse eyes due to the small eye size (about 3.2 mm diameter; 5 μL in volume) and high intraocular pressure (IOP) after injection (Figure 1). As these factors play out at the microscale during implantation, solid sample loading and injection are made increasingly difficult. These technical limitations have prevented testing of ODIs in the large number of available mouse models for eye disease (White et al., 2013).

Here, we describe a simple, cost-effective, robust, and minimally invasive intravitreal injection method to deliver ODIs into mouse eyes, which we call "mouse implant intravitreal injection" (MI3).

RESULTS

Micro-scaled ocular drug implants designed for mouse show sustained drug release *in vitro*

Implant formulation holds advantages in sustained drug release, and it is especially beneficial to overcome pharmacokinetic limitations of hydrophobic drugs under physiologic conditions due to their insolubility or heterogeneity. However, it is not well understood whether micro-scaled ocular implants, in the size suitable for mouse injection, retain pharmacokinetic advantages. To address this, we formulated micro-scaled implants (50–80 μm in diameter and 500–2,000 μm in length) containing a hydrophobic model drug (cyanine 5.5 [Cy5.5], molecular weight [MW] 619.23 Da). A biodegradable polymer widely used for controlled drug release, poly lactic-co-glycolic acid (PLGA), was mixed with Cy5.5 at a weight ratio of 95 to 5 resulting in a Cy5.5-PLGA implant (dark blue color under white light; Figure S1A). In phosphate-buffered saline (PBS) supplemented with 0.1% (w/v) bovine serum albumin (BSA), the Cy5.5-PLGA implant showed sustained release of the model drug (Figure S1B). This indicated that micro-scaled drug implants may have the pharmacokinetic advantages of implant formulation.

MI3 method can inject implants into small-sized mouse eyes

ODIs have largely been tested using *in vivo* models with eyes much larger than mice (e.g., rabbits or non-human primates). In these larger-eyed animal models, ODIs were typically introduced into eyes through 1-mm-wide incisions (Al-Nawaiseh et al., 2016). However, this procedure is too invasive and damaging to be applied to mouse eyes, which average only 3.2 mm in diameter (Figure 1). With conventional needle-based intravitreal injection tools and methods, drugs that can be stably suspended or emulsified in liquid solutions (soluble or colloidal drugs) are robustly and safely injected into mouse eyes, yet monolithic drug depots such as implants are not injectable due to their relatively strict physical properties such as size and shape. Thus, we sought to develop an intravitreal implant administration tool (MI3) that retains the safety of conventional needle-based intravitreal injection methods but is not limited by the physical properties of implants.

Considering the microscopic size and hair-like properties needed for mouse ODIs, we hypothesized that the intravitreal injection methods currently in use for soluble and colloidal ocular drugs may be adapted to inject solid ODIs into mouse eyes. Conventionally, commercially available, small-gauge stainless-steel needles or glass capillary needles made in laboratories were utilized for intravitreal injection of drugs to mouse eyes. Compared with small-gauge stainless-steel needles, glass capillary needles may be advantageous for the intravitreal injection of implants. The dimensions and properties of glass capillary needles can be easily adjusted and modified depending on the properties of implants under different experimental setups. The

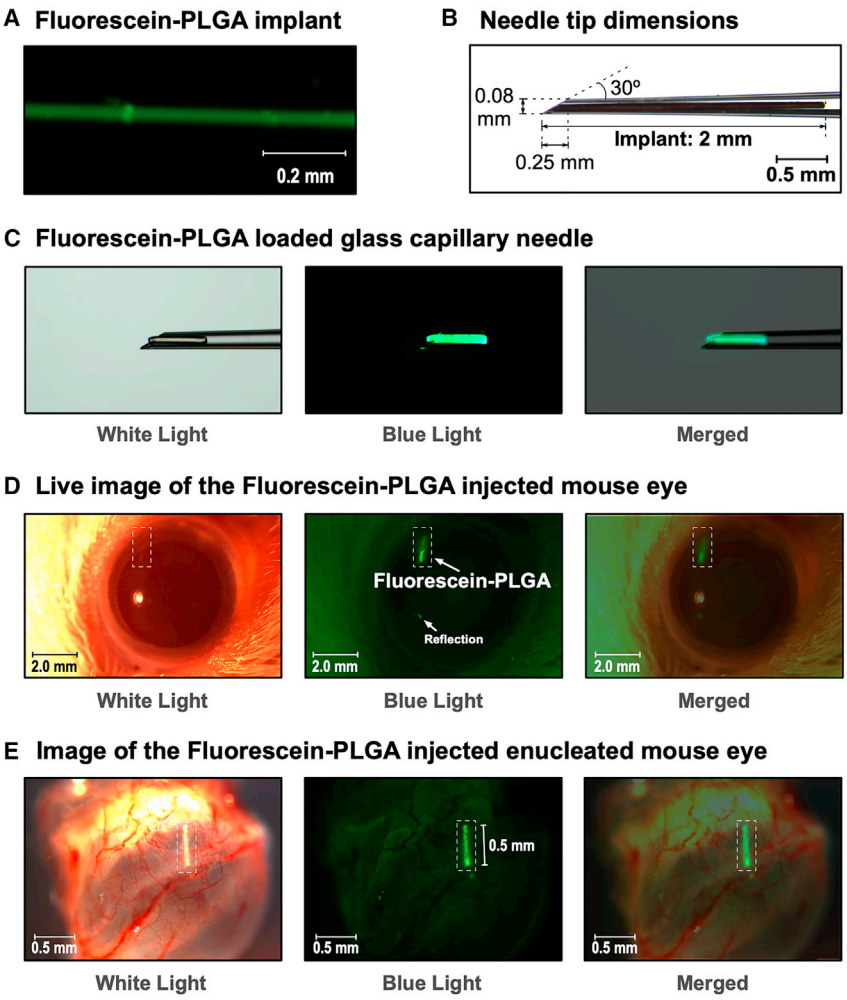

Figure 2. Ocular implants can be successfully injected into small-sized mouse eyes by MI3 method

(A) Fluorescein-PLGA implant fluoresces green under blue light.

(B) Implant-loaded glass capillary needle and its dimensions.

(C) A fluorescein-PLGA-loaded needle is shown under white light, blue light, and merged.

(D) Live image of mouse eye injected with the 0.5-mm fluorescein-PLGA implant. Fluorescein-PLGA particle can be observed under both white and blue light.

(E) Fluorescein-PLGA-injected mouse eye was enucleated, and it was tissue-cleared using PACT method. Fluorescein-PLGA was observable under both white and blue light through cleared sclera.

transparency of glass capillary needles also allows easy visual examination of implants in needles. Thus, we built on previously established methods of intravitreal injection in mice, which utilize glass capillary needles, to load an implant (Chan et al., 2020; Wang et al., 2014; Wert et al., 2012). We followed the capillary fabrication procedure that involved heating the middle section of a borosilicate glass capillary and stretching it with a micropipette puller to achieve an inner diameter of 50–100 μm (Figure S2A, panels 1–5), and then polished it to a 30-degree angle for optimal sclera penetration, resulting in an intravitreal injection needle (Figure S2A, panels 6 and 7). To load the solid implant into the needle, we devised a method using forceps to insert the implant into the needle tip (Figure S2A, panels 8 and 9) and filled the needle with a PBS buffer to keep air from entering the vitreous upon injection (Figure S2A, panels 10 and 11). To demonstrate the robustness, safety, and experimental application potentials of our MI3 method, we used fluorescein-labeled PLGA implants (green color under blue light; fluorescein-PLGA and PLGA mixture at a weight ratio of 1:10; Figure 2A) and were able to load the implants into the glass capillary needles (Figures 2B and 2C).

We first tested whether conventional Hamilton-syringe-based intravitreal injection that manually generates pressure to inject the implant was possible and found that the implant could be injected. For more robust control of injection parameters (e.g., applied pressure and injection duration), an electronic microinjector could be more advantageous (Figures S2B–S2E). The injection pressure and time of the electronic microinjector were optimized for the implant (500 hPa injection pressure, 1.0 s injection time). Even though the surgical setup and procedure were straightforward, we found that the electronic microinjector might be limited in certain implant sizes and surface resistance.

To develop a more versatile injection method that could accommodate implants with more varied characteristics, we developed a plunger-based approach to physically push the implant out of the needle rather than utilizing air pressure. We ground a syringe-cleaning wire to a diameter of 50 μm with a whetstone to create the implant plunger (Figure S3A) and assembled it at the opposite end of the needle tip and implant (Figure S3B). A micromanipulator was used to insert the needle into the eye at a 30° angle (Figures S3C and S3D), and the plunger was then used to gently push out the implant (Video S1). During injection, as the implant went into the vitreous, a small volume of vitreous fluid flowed back into the needle, likely to compensate for the implant volume and to maintain proper intraocular pressure (Video S1). While more involved, we found that implant injection by plunger could accommodate implants of a greater range of sizes (up to 2 mm), shapes, and surface resistances.

Immediately after the implant injection, the ODI-injected mouse eyeball was examined. The injected fluorescein-PLGA implant was clearly observable in the live image and enucleated eye image (cleared by passive clarity technique [PACT] method; Treweek et al., 2015) was taken under fluorescence microscope (Figures 2D and 2E). No sign of severe trauma (e.g., intravitreal

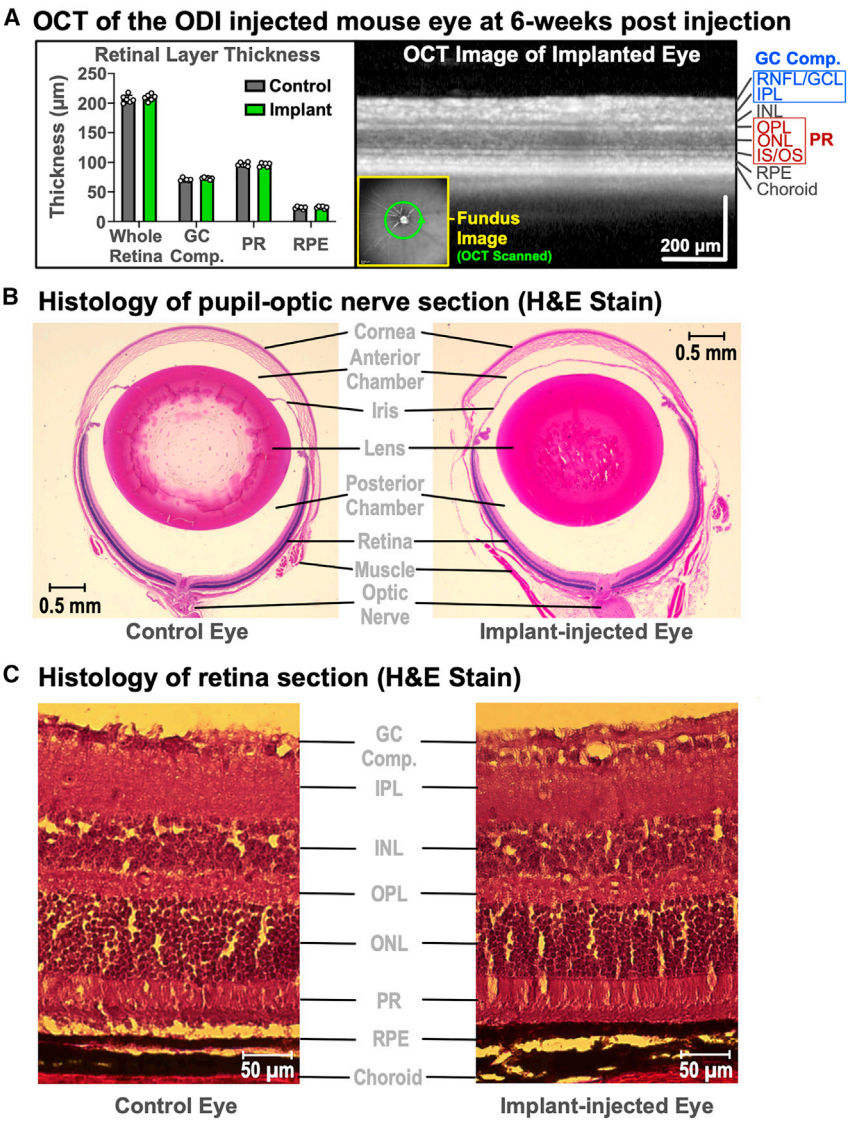

Figure 3. MI3 method does not disrupt retinal structure of implant-injected mouse eyes

(A) Spectral domain optical coherence tomography (SD-OCT) shows that there is no significant difference in retinal structures between the control eye and implant-injected eye at 6 weeks post injection (n = 6 for each group). Infrared scanning laser ophthalmoscope (SLO; yellow box) and OCT (right panel) images of an implant-injected eye are shown. Green lines on infrared SLO image indicate the regions where OCT images were taken.

(B) Representative images of pupil-optic nerve section (n = 4 for each group). No significant difference was observed between control and implant-injected eyes. Compared with control eyes (left), no significant difference was observed in implant-injected eyes (right).

(C) Representative images of retina section. Retinas were detached from eye and sectioned for imaging. Histologic analysis of retina sections shows no significant difference between control and implant-injected eye, and it confirms that there are no signs of inflammation or cell death (n = 6 for each group).

hemorrhages, cataract, or sclera damage) was observed under the microscope. After 6 weeks of a 0.5-mm PLGA implant injection (n = 6), the PLGA implants were no longer present in the mouse vitreous, likely indicating biodegradation of PLGA implants.

Anatomical and physiological examinations of ODI-injected mouse eyes suggest that MI3 method does not damage the eyes

Spectral domain optical coherence tomography (SD-OCT) is a powerful and commonly used non-invasive *in vivo* live imaging technique used to characterize and examine the structure of the retina. We tested whether these imaging techniques could provide quality data in the ODI-injected mouse eyes. We took SD-OCT of the control (no injection) eyes and the 0.5-mm PLGA-implant-injected eyes at 6 weeks post injection (n = 6 for each group). Implants in the vitreous did not interfere with the retina imaging by the SD-OCT. Compared with the control eyes, implant-injected eyes did not show any significant structural or thickness changes in the retinal layers (Figure 3A). We further investigated whether the procedure induced any complications by examining the hematoxylin and eosin (H&E) histology of pupil-optic nerve sections (Figure 3B) and retina sections of the eyes (Figure 3C). There was no cataract, vitreous hemorrhage, intraocular inflammation, or retinal cell death on gross exam or by histology in ten mouse eyes injected with varying sizes (0.5–2.0 mm) of implants compared to control eyes. As expected, there was minor tissue damage only at the needle entry site. This suggests that the surgical procedure does not damage the retinal structure and gross anatomy, and non-invasive retina imaging methods can be utilized to track the retina structures to address ODI efficacy and toxicity over time in mouse eyes. Thus, the MI3 implant delivery method can allow noninvasive studies of controlled release ODIs in mouse models.

Electroretinograms of ODI-injected mouse eyes suggest that MI3 method does not damage the retinal functions

We further evaluated the implant-injected mouse eyes with electroretinography (ERG) to address whether the surgery affected retinal function in mice. ERG is an *in vivo* technique that measures the electrical responses of retinal cells such as ganglion cells, inner retinal cells, and photoreceptors and indicates physiological health. It is a non-invasive method that is widely used to test the function of the retina in humans and mouse models. The normal retina shows very distinctive electrical response patterns: an initial negative electric amplitude spike, called an a-wave,

CellPress
OPEN ACCESS

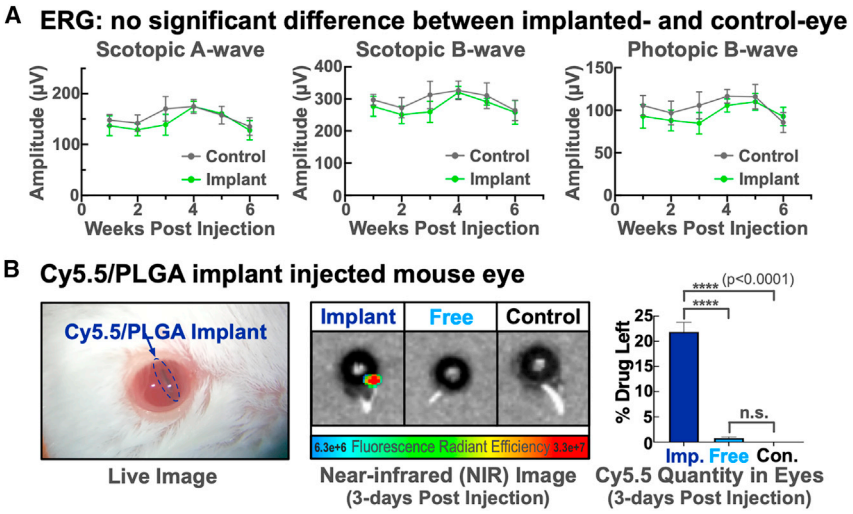

Figure 4. MI3 method does not disrupt retinal function of implant-injected mouse eyes, and the implant sustainedly releases drug *in vivo*

(A) Electroretinography comparison of the scotopic 1.0 global ERG and photopic 3.0 (flash strength in cd.s.m^{-2}) in implant-injected eyes and no-injection control eyes (n = 6 for each group). No significant difference was observed between control and test groups.

(B) Left panel: live image of albino-mouse eye injected with the 2-mm Cy5.5-PLGA implant taken right after the surgery. Cylinder-shaped dark blue object (Cy5.5-PLGA) can be clearly observed through mouse lens. Middle panel: near-infrared (NIR) image of enucleated eyes with Cy5.5-PLGA implant, free Cy5.5 solution, and no injection control. Strong NIR fluorescence signal was detected in implant-injected eye, whereas other eyes did not show any NIR signals. This suggests that model drug was washed out from eye within 3 days, whereas the implant prolonged drug retention time in mouse vitreous. Right panel: the amount of remaining Cy5.5 in eyes at 3 days post injection was quantified (minimum n = 4 for each group; data displayed as mean ± SEM). Implant-injected eyes had significant amounts of drug left compared to free-Cy5.5-injected or control groups (****: p < 0.0001). There was no significant difference between free-Cy5.5-injected and control groups.

followed by a positive electric amplitude spike, called a b-wave. For the control wild-type C57BL/6J mice, the average a-wave is −150 μV and the b-wave is 300 μV in scotopic 1.0 (flash strength in cd.s.m^{-2}) measures. We performed weekly ERG measures of the control (no injection) eyes and the 0.5-mm PLGA-implant-injected eyes for 6 weeks after injection (n = 6 for each group). There were no significant differences in the ERG responses between the control group and the test group. The ERG responses remained stable and normal for 6 weeks post implant injection (Figure 4A). This suggests that our surgery method does not damage the retinal physiological function, and the ERG method can be used as a functional measure to address the efficacy and toxicity of ODIs in mouse eyes.

Sustained release of a model drug implant in mouse eyes: Infrared imaging and model drug quantification in mouse eyes

After confirming the robustness, safety, and utility of the MI3 method, we injected Cy5.5/PLGA implants into mouse eyes to determine whether the pharmacokinetic advantages of mouse ODIs we observed *in vitro* persisted *in vivo*. Either the Cy5.5-PLGA implant or non-formulated (free) Cy5.5 was intravitreally injected into the eyes of a group of six or four mice, respectively, along with a no-drug-injected control mouse group (n = 4). The injected Cy5.5/PLGA implant was clearly observable through the mouse lens under a dissecting microscope just after injection (Figure 4B, left panel). At 3 days post injection, the eyes were enucleated, and the remaining intraocular drug was measured by non-invasive near-infrared (NIR) image analysis and drug quantification in protease-digested samples (Figure 4B, middle panel). A strong NIR fluorescent signal was detected in the implant-injected eyes, and about 22% of the initial dose remained. This release appeared to be faster than *in vitro* (Figure S1B), which may be due to dynamic compositional differences in the vitreous. NIR signals were not detectable in either the free-Cy5.5-injected or control eyes. The free-Cy5.5-injected eyes had no significant difference in the remaining drug amount compared with the control (no drug) eyes (Figure 4B, right panel). Therefore, there was rapid clearance of free-Cy5.5 within 3 days, whereas the implant formulation prolonged drug retention time in the mouse eyes. The implant formulation strategy retained its pharmacokinetic advantages in mice. This suggests that in future experiments, different small molecules conjugated to ODIs can be tested in various mouse eye disease models for therapeutic outcomes.

DISCUSSION

An intraocular drug implant is an attractive drug formulation strategy for controlled release within the eye. Even though small molecule drugs hold many advantages, such as high potency and specificity, scalable and efficient drug manufacturing, and stability during drug storage and distribution, a major disadvantage in an ocular environment is the fast vitreous-clearance rate (e.g., half-life of dexamethasone in the vitreous is about 5.5 h; Gan et al., 2005) resulting in a short efficacious period and the need for more frequent administration. The formulation of small molecule drugs into intraocular drug implants can overcome these disadvantages, since implants have been designed to release drugs in the vitreous at a slow, sustained rate over extended periods of time, greatly reducing the frequency of dosing required. The implant formulation can be optimized to load high amounts of sequestered drug in a drug depot, which avoids exposing eyes to high drug doses. Releasing drugs in the vitreous via scaffold degradation and/or drug diffusion could potentially lead to toxicity and off-target effects. Instead, ODIs serve as a reservoir that releases drugs over time. They do not require direct chemical modifications of drugs, therefore avoiding reduction in drug efficacy from the irreversible alteration in drug structure, previously observed in ranibizumab

(Campochiaro et al., 2019). Once the efficacious drug composition and dosage are defined, an implant can be designed and developed by optimizing matrix stability, drug release kinetics, and the functionality of a post-release drug. This optimization step includes the selection of implant materials (Stewart et al., 2018). The pharmacokinetic advantages of ocular drug implants and the slow, sustained release of drugs over extended periods of time are especially beneficial for treating and preventing accumulative and slow-progressing chronic retinal diseases, such as age-related macular degeneration, diabetic retinopathy, and retinitis pigmentosa.

There are many other ocular disease animal models with small eyes (less than 10 mm diameter), such as zebrafish (Richardson et al., 2017), newts (Islam et al., 2014), xenopus (Pfirrmann et al., 2015), lizards (Pérez i de Lanuza et al., 2018), and chicks (Wisely et al., 2017), that are used extensively in vision research. Even though these small-eyed animals are abundant and provide robust model systems to test drug efficacy, ocular drug implant studies can be difficult in these species because there are no good methods to deliver ocular drug implants into animals with small eyes. Thus, efficacy testing and optimization of ODIs are typically carried out in animals with larger eyes, such as rabbit or pig, which are more expensive and have limited disease models compared to small animals. We have shown that our MI3 method is a robust and effective method to deliver ocular implants to small mouse eyes. This method can deliver solid implants of varying sizes and holds all the advantages of conventional intravitreal injection methods for small-eyed model animals. We have also demonstrated that the injected mouse eyes can be examined with non-invasive *in vivo* imaging methods (Figures 3A and 4A). This is important to monitor the structure and function of the eye, which can serve as measures for drug efficacy and toxicity. Colloidal formulation (e.g., hydrogel and nanoparticles) or dendrimer-based formulation techniques have been utilized for controlled release of ocular drugs and have been tested in mice via conventional intravitreal injection method (Delplace et al., 2019; Huang and Chau, 2019; Kambhampati et al., 2015). Our MI3 method expands the mouse-testable formulation options for ocular drugs by including solid implants. Considering that the products with colloidal and dendrimer-based formulations exhibit limited homogeneity and stability, solid implants may have very unique advantages, such as highly defined and homogeneous physical and chemical properties.

Micron-sized mouse implants can release drugs faster than millimeter-sized human implants due to their relatively larger surface-area-to-volume ratios. Further optimization of mouse implants, such as modifying implant surfaces or using different polymer compositions, may be needed to obtain suitable drug release profiles (Chen et al., 2018; Hines and Kaplan, 2013). A recent study demonstrated that microneedles made up of PLGA and PLA created for humans, which exhibit similar geometric values to mouse implants, show a sustained release of a drug for two months (Li et al., 2019). Thus, the pharmacokinetics of this appropriately sized mouse drug implant will need to be evaluated further in the context of a larger human eye. However, testing implants in mouse eyes will provide data on efficacy and toxicity of a sustained release drug, which will serve as target reference parameters when developing human ocular implants. This ocular implant testing platform in mice will also be beneficial for rediscovering drug candidates that were effective *in vitro*, but not efficacious *in vivo* due to their very short residing time or stability in the vitreous. Various ocular drugs, such as antiviral, antifungal, and antibiotic small molecule drugs (e.g., vancomycin, amphotericin B, and trifluorothymidine) (Ahn et al., 2013), steroids (e.g., dexamethasone, triamcinolone acetonide, and fluocinolone acetonide) (Sarao et al., 2014), immunosuppressants (e.g., methotrexate) (Frenkel et al., 2008), or anti-angiogenic compounds (e.g., genistein) (Keum et al., 2020; Li et al., 2020; Sulaiman et al., 2016), can be applied using the implant system to enhance their therapeutic efficiency while reducing local and systemic toxicity and off-target effects.

Our injection technique can be used to develop novel therapeutics as well as to determine pathogenesis of posterior segment eye diseases. This method enables further preclinical characterization of ODIs in small rodent animal models. In addition, this method holds high potential to generate new animal models for chronic eye diseases, which are caused by sustained exposures to disease-inducing toxins and pathogens, by using implants loaded with disease-inducing small molecules. Since this technique enables an implant with a toxin or pathogen to be directly injected into the vitreous humor, targeted delivery of pathogens is expected and can parse out the eye-specific pathogenic mechanism from other systemic pathogenic mechanisms.

In conclusion, we present a robust intraocular implant injection technique (MI3) for small animal models. This method can be used to inject appropriately sized monolithic ocular drug implants with sustained release into the vitreous of mice in a safe and efficacious manner. Future studies utilizing this technique can be used for drug screening and disease modeling.

Limitations of the study

Our method allows for the testing of small molecule implants in a broad range of ocular disease mouse models to determine efficacy, toxicity, and desired drug dose and release rates. However, the implant's dimensions are not directly scalable from micron-sized mouse implants to millimeter-sized human implants, considering that a smaller particle leads to a faster release rate due to the surface-area-to-volume ratio. Thus, based on the efficacious dose, release rate, and toxicity parameters identified in mouse models, implants may require formulation optimization in animal models with human-sized eyes.

The length of an implant will be limited by the axial length of the mouse eye (3.2 mm; Figure 1A), and the diameter of an implant will be limited by the inner diameter of the intravitreal injection needle (80–100 μm; Figure 2B). The MI3 method can inject up to a 2-mm-long (axial length of mouse eye) flexible implant into the mouse vitreous, yet a smaller implant that provides sufficient drug may be preferable for better safety and less potential tissue damage. Based on the physical properties of the implants (size, weight, density, and surface property), either an electronic microinjector (Figures S2B–S2E) or a plunger (Figure S3) can be used. The electronic microinjector method is easier to use than the plunger-based method, but smaller, lighter, and/or less surface-resistant implants are preferred. The plunger-based

method is less restricted from the physical properties of implants. For experienced users, we recommend testing the electronic microinjector method first due to the simple surgical setup and procedure.

STAR★METHODS

Detailed methods are provided in the online version of this paper and include the following:

- KEY RESOURCES TABLE
- RESOURCE AVAILABILITY
  - Lead contact
  - Materials availability
  - Data and code availability
- EXPERIMENTAL MODEL AND SUBJECT DETAILS
  - Mice
- METHOD DETAILS
  - *In vitro* release profiling of a model drug implant (Cy5.5/PLGA)
- QUANTIFICATION AND STATISTICAL ANALYSIS

SUPPLEMENTAL INFORMATION

Supplemental information can be found online at https://doi.org/10.1016/j.crmeth.2021.100125.

ACKNOWLEDGMENTS

We thank Dr. Jeffrey Goldberg in the department of ophthalmology at Stanford University for allowing us to use his micromanipulator for plunger-based implant injections. We thank Drs. Michael Kapiloff and Jinliang Li in the department of ophthalmology at Stanford University for training and allowing us to use their microscope to collect histology images. We thank Drs. Liang Li, Gabriella Maria Fernandes Cunha, and David Myung in the department of ophthalmology at Stanford University for helpful discussions. We also thank Dr. Jill Helms in the department of surgery at Stanford University for allowing us to use her teaching microscope to collect videos and images for the procedure. V.B.M. is supported by NIH grants (R01EY026682, R01EY024665, R01EY025225, R01EY024698, and P30EY026877), Stanford ChEM-H IMA, the Stanford Center for Optic Disc Drusen, and Research to Prevent Blindness, New York, New York. S.W. is supported by American Diabetes Association (1-16-INI-16), NIH grants (R01NS109990 and 1R01EY03258501), and P30 to Stanford Ophthalmology. YJS is supported by BrightFocus Foundation's Macular Degeneration Research program. The contents of this publication are solely the responsibility of the authors and do not necessarily represent the official views of the sponsor.

AUTHOR CONTRIBUTIONS

Study concept and design, V.B.M.; acquisition of data, Y.J.S., C.H.L., M.R.W., S.H.L., J.Y., and C.R.K.; data analysis and interpretation, Y.J.S., C.H.L., M.R.W., S.H.L., J.Y., C.R.K., S.W., and V.B.M.; drafting of the manuscript and video, Y.J.S., C.H.L., M.R.W., S.H.L., J.Y., C.R.K., E.M.M., Y.S.J., S.W., and V.B.M.; critical revision of the manuscript, Y.J.S., C.H.L., S.H.L., E.M.M., B.C., S.W., and V.B.M.; obtained funding, S.W. and V.B.M.; administrative, technical, and material support, V.B.M.; study supervision, V.B.M.

DECLARATION OF INTERESTS

The authors declare no competing interests.

INCLUSION AND DIVERSITY

One or more of the authors of this paper self-identifies as an underrepresented ethnic minority in science.

Received: June 24, 2021
Revised: September 15, 2021
Accepted: November 12, 2021
Published: December 6, 2021

REFERENCES

Ahn, J., Kim, H., Woo, S.J., Park, J.H., Park, S., Hwang, D.J., and Park, K.H. (2013). Pharmacokinetics of intravitreally injected bevacizumab in vitrectomized eyes. J. Ocul. Pharmacol. Ther. *29*, 612–618. https://doi.org/10.1089/jop.2013.0009.

Al-Nawaiseh, S., Thieltges, F., Liu, Z., Strack, C., Brinken, R., Braun, N., Wolschendorf, M., Maminishkis, A., Eter, N., and Stanzel, B.V. (2016). A step by step protocol for subretinal surgery in rabbits. JoVE *115*, 53927. https://doi.org/10.3791/53927.

Campochiaro, P.A., Marcus, D.M., Awh, C.C., Regillo, C., Adamis, A.P., Bantseev, V., Chiang, Y., Ehrlich, J.S., Erickson, S., Hanley, W.D., et al. (2019). The port delivery system with ranibizumab for neovascular age-related macular degeneration: results from the randomized phase 2 ladder clinical trial. Ophthalmology *126*, 1141–1154. https://doi.org/10.1016/j.ophtha.2019.03.036.

Chames, P., Van Regenmortel, M., Weiss, E., and Baty, D. (2009). Therapeutic antibodies: successes, limitations and hopes for the future. Br. J. Pharmacol. *157*, 220–233. https://doi.org/10.1111/j.1476-5381.2009.00190.x.

Chan, C.S.Y., Lonfat, N., Zhao, R., Davis, A.E., Li, L., Wu, M.-R., Lin, C.-H., Ji, Z., Cepko, C.L., and Wang, S. (2020). Cell type- and stage-specific expression of Otx2 is regulated by multiple transcription factors and cis-regulatory modules in the retina. Development *147*, dev187922. https://doi.org/10.1242/dev.187922.

Chen, W., Yung, B.C., Qian, Z., and Chen, X. (2018). Improving long-term subcutaneous drug delivery by regulating material-bioenvironment interaction. Adv. Drug Deliv. Rev. *127*, 20–34. https://doi.org/10.1016/j.addr.2018.01.016.

Delplace, V., Ortin-Martinez, A., Tsai, E.L.S., Amin, A.N., Wallace, V., and Shoichet, M.S. (2019). Controlled release strategy designed for intravitreal protein delivery to the retina. J. Contr. Release *293*, 10–20. https://doi.org/10.1016/j.jconrel.2018.11.012.

El-Ghrably, I.A., Saad, A., and Dinah, C. (2015). A novel technique for repositioning of a migrated ILUVIEN(®) (fluocinolone acetonide) implant into the anterior chamber. Ophthalmol. Ther. *4*, 129–133. https://doi.org/10.1007/s40123-015-0035-1.

Frenkel, S., Hendler, K., Siegal, T., Shalom, E., and Pe'er, J. (2008). Intravitreal methotrexate for treating vitreoretinal lymphoma: 10 years of experience. Br. J. Ophthalmol. *92*, 383–388. https://doi.org/10.1136/bjo.2007.127928.

Gan, I.M., Ugahary, L.C., van Dissel, J.T., and van Meurs, J.C. (2005). Effect of intravitreal dexamethasone on vitreous vancomycin concentrations in patients with suspected postoperative bacterial endophthalmitis. Graefe's Arch. Clin. Exp. Ophthalmol. *243*, 1186–1189. https://doi.org/10.1007/s00417-005-1182-1.

Haller, J.A., Bandello, F., Belfort, R., Jr., Blumenkranz, M.S., Gillies, M., Heier, J., Loewenstein, A., Yoon, Y.H., Jacques, M.L., Jiao, J., et al. (2010). Randomized, sham-controlled trial of dexamethasone intravitreal implant in patients with macular edema due to retinal vein occlusion. Ophthalmology *117*, 1134–1146.e3. https://doi.org/10.1016/j.ophtha.2010.03.032.

Hines, D.J., and Kaplan, D.L. (2013). Poly(lactic-co-glycolic) acid–controlled-release systems: experimental and modeling insights. Crit. Rev. Ther. Drug Carrier Syst. *30*, 257–276. https://doi.org/10.1615/CritRevTherDrugCarrierSyst.2013006475.

Horio, N., Kachi, S., Hori, K., Okamoto, Y., Yamamoto, E., Terasaki, H., and Miyake, Y. (2001). Progressive change of optical coherence tomography scans

in retinal degeneration slow mice. Arch. Ophthalmol. *119*, 1329–1332. https://doi.org/10.1001/archopht.119.9.1329.

Huang, X., and Chau, Y. (2019). Intravitreal nanoparticles for retinal delivery. Drug Discov. Today *24*, 1510–1523. https://doi.org/10.1016/j.drudis.2019.05.005.

Islam, M.R., Nakamura, K., Casco-Robles, M.M., Kunahong, A., Inami, W., Toyama, F., Maruo, F., and Chiba, C. (2014). The newt reprograms mature RPE cells into a unique multipotent state for retinal regeneration. Sci. Rep. *4*, 6043. https://doi.org/10.1038/srep06043.

Kambhampati, S.P., Clunies-Ross, A.J.M., Bhutto, I., Mishra, M.K., Edwards, M., McLeod, D.S., Kannan, R.M., and Lutty, G. (2015). Systemic and intravitreal delivery of dendrimers to activated microglia/macrophage in ischemia/reperfusion mouse retina. Invest. Ophthalmol. Vis. Sci. *56*, 4413–4424. https://doi.org/10.1167/iovs.14-16250.

Keum, D.H., Kim, S.K., Koo, J., Lee, G.H., Jeon, C., Mok, J.W., Mun, B.H., Lee, K.J., Kamrani, E., Joo, C.K., et al. (2020). Wireless smart contact lens for diabetic diagnosis and therapy. Sci. Adv. *6*, eaba3252. https://doi.org/10.1126/sciadv.aba3252.

Li, W., Terry, R.N., Tang, J., Feng, M.R., Schwendeman, S.P., and Prausnitz, M.R. (2019). Rapidly separable microneedle patch for the sustained release of a contraceptive. Nat. Biomed. Eng. *3*, 220–229. https://doi.org/10.1038/s41551-018-0337-4.

Li, Y., Alhendi, A.M.N., Yeh, M.C., Elahy, M., Santiago, F.S., Deshpande, N.P., Wu, B., Chan, E., Inam, S., Prado-Lourenco, L., et al. (2020). Thermostable small-molecule inhibitor of angiogenesis and vascular permeability that suppresses a pERK-FosB/ΔFosB-VCAM-1 axis. Sci. Adv. *6*, eaaz7815. https://doi.org/10.1126/sciadv.aaz7815.

Mahajan, V.B., Skeie, J.M., Assefnia, A.H., Mahajan, M., and Tsang, S.H. (2011). Mouse eye enucleation for remote high-throughput phenotyping. JoVE *57*, 3184. https://doi.org/10.3791/3184.

Maya-Vetencourt, J.F., Manfredi, G., Mete, M., Colombo, E., Bramini, M., Di Marco, S., Shmal, D., Mantero, G., Dipalo, M., Rocchi, A., et al. (2020). Subretinally injected semiconducting polymer nanoparticles rescue vision in a rat model of retinal dystrophy. Nat. Nanotechnol. *15*, 698–708. https://doi.org/10.1038/s41565-020-0696-3.

Moisseiev, E., Regenbogen, M., Rabinovitch, T., Barak, A., Loewenstein, A., and Goldstein, M. (2014). Evaluation of pain during intravitreal Ozurdex injections vs. intravitreal bevacizumab injections. Eye (London, England) *28*, 980–985. https://doi.org/10.1038/eye.2014.129.

Parsons, D.E., Lee, S.H., Sun, Y.J., Velez, G., Bassuk, A.G., Smith, M., and Mahajan, V.B. (2021). Peptidomimetics therapeutics for retinal disease. Biomolecules *11*, 339. https://doi.org/10.3390/biom11030339.

Pfirrmann, T., Emmerich, D., Ruokonen, P., Quandt, D., Buchen, R., Fischer-Zirnsak, B., Hecht, J., Krawitz, P., Meyer, P., Klopocki, E., et al. (2015). Molecular mechanism of CHRDL1-mediated X-linked megalocornea in humans and in Xenopus model. Hum. Mol. Genet. *24*, 3119–3132. https://doi.org/10.1093/hmg/ddv063.

Pérez i de Lanuza, G., Ábalos, J., Bartolomé, A., and Font, E. (2018). Through the eye of a lizard: hue discrimination in a lizard with ventral polymorphic coloration. J. Exp. Biol. *221*, jeb169565. https://doi.org/10.1242/jeb.169565.

Richardson, R., Tracey-White, D., Webster, A., and Moosajee, M. (2017). The zebrafish eye—a paradigm for investigating human ocular genetics. Eye *31*, 68–86. https://doi.org/10.1038/eye.2016.198.

Sarao, V., Veritti, D., Boscia, F., and Lanzetta, P. (2014). Intravitreal steroids for the treatment of retinal diseases. ScientificWorldJournal *2014*, 989501. https://doi.org/10.1155/2014/989501.

Schmucker, C., and Schaeffel, F. (2004). A paraxial schematic eye model for the growing C57BL/6 mouse. Vis. Res. *44*, 1857–1867. https://doi.org/10.1016/j.visres.2004.03.011.

Shmueli, R.B., Ohnaka, M., Miki, A., Pandey, N.B., Lima e Silva, R., Koskimaki, J.E., Kim, J., Popel, A.S., Campochiaro, P.A., and Green, J.J. (2013). Long-term suppression of ocular neovascularization by intraocular injection of biodegradable polymeric particles containing a serpin-derived peptide. Biomaterials *34*, 7544–7551. https://doi.org/10.1016/j.biomaterials.2013.06.044.

Stewart, S.A., Domínguez-Robles, J., Donnelly, R.F., and Larrañeta, E. (2018). Implantable polymeric drug delivery devices: classification, manufacture, materials, and clinical applications. Polymers *10*, 1379. https://doi.org/10.3390/polym10121379.

Sulaiman, R.S., Merrigan, S., Quigley, J., Qi, X., Lee, B., Boulton, M.E., Kennedy, B., Seo, S.Y., and Corson, T.W. (2016). A novel small molecule ameliorates ocular neovascularisation and synergises with anti-VEGF therapy. Sci. Rep. *6*, 25509. https://doi.org/10.1038/srep25509.

Treweek, J.B., Chan, K.Y., Flytzanis, N.C., Yang, B., Deverman, B.E., Greenbaum, A., Lignell, A., Xiao, C., Cai, L., Ladinsky, M.S., et al. (2015). Whole-body tissue stabilization and selective extractions via tissue-hydrogel hybrids for high-resolution intact circuit mapping and phenotyping. Nat. Protoc. *10*, 1860–1896. https://doi.org/10.1038/nprot.2015.122.

Uddin, F., Rudin, C.M., and Sen, T. (2020). CRISPR gene therapy: applications, limitations, and implications for the future. Front. Oncol. *10*, 1387.

Wang, S., Sengel, C., Emerson, Mark M., and Cepko, Constance L. (2014). A gene regulatory network controls the binary fate decision of rod and bipolar cells in the vertebrate retina. Dev. Cell *30*, 513–527. https://doi.org/10.1016/j.devcel.2014.07.018.

Wert, K.J., Skeie, J.M., Davis, R.J., Tsang, S.H., and Mahajan, V.B. (2012). Subretinal injection of gene therapy vectors and stem cells in the perinatal mouse eye. JoVE *69*, e4286. https://doi.org/10.3791/4286.

White, J.K., Gerdin, A.K., Karp, N.A., Ryder, E., Buljan, M., Bussell, J.N., Salisbury, J., Clare, S., Ingham, N.J., Podrini, C., et al. (2013). Genome-wide generation and systematic phenotyping of knockout mice reveals new roles for many genes. Cell *154*, 452–464. https://doi.org/10.1016/j.cell.2013.06.022.

Wisely, C.E., Sayed, J.A., Tamez, H., Zelinka, C., Abdel-Rahman, M.H., Fischer, A.J., and Cebulla, C.M. (2017). The chick eye in vision research: an excellent model for the study of ocular disease. Prog. Retin. Eye Res. *61*, 72–97. https://doi.org/10.1016/j.preteyeres.2017.06.004.

STAR★METHODS

KEY RESOURCES TABLE

REAGENT or RESOURCE	SOURCE	IDENTIFIER
Chemicals, peptides, and recombinant proteins		
AnaSed® xylazine injection	Akorn Inc, Lake Forest, IL, USA	NDC: 59399-110-20
Cyanine5.5 carboxylic acid	Lumiprobe Corporation, Hunt Valley, MD, USA	Cat. #: 47090
Eosin Y	Fisher Scientific, Hampton, NH, USA	Item #: 17372-87-1
Gill III Hematoxylin	Mercedes Scientific, Lakewood Ranch, FL, USA	Item #: MER 347961GL
Phloxine B	Electron Microscopy Sciences, Hatfield, PA, USA	Item #: 19350
Poly(D,L-lactide-*co*-glycolide)	Sigma Aldrich Inc, St. Louis, MO	SKU: P2191
Poly(lactide-co-glycolide)-Fluorescein	Sigma Aldrich Inc, St. Louis, MO	SKU: 908649-50MG
Refresh Liquigel® Lubricant Eye Gel	Allergan, Irvine, CA, USA	NDC: 0023-9205
Tissue-Tek® O.C.T. Compound	VWR International, LLC, Radnor, PA, USA	Cat. #: 4583
Tropicamide ophthalmic solution (1%)	Akorn Inc, Lake Forest, IL, USA	NDC: 17478-102-12
VetaKet® CIII (ketamine hydrochloride injection, USP)	Akorn Inc, Lake Forest, IL, USA	NDC: 59399-114-10
Experimental models: Organisms/strains		
Mouse: WT BALB/c	Envigo, USA	N/A
Mouse: WT C57BL/6J	The Jackson Laboratory, USA	Stock #: 000664
Software and algorithms		
Aura imaging software	Spectral Instruments Imaging, Tuscon, AZ, USA	https://spectralinvivo.com/
GraphPad Prism 8	GraphPad Software, Inc.	https://www.graphpad.com/
ImageJ	National Institutes of Health (NIH)	https://imagej.nih.gov/ij/index.html
Leica Application Suite X	Leica Microsystems, San Francisco, CA, USA	https://www.leica-microsystems.com/products/microscope-software/p/leica-las-x-ls/
Other		
Black Arkansas stone	Dan's Whetstone Company Inc., AR, USA	N/A
Borosilicate glass capillaries	World Precision Instruments, FL, USA	Cat. #: 1B100-4
Capillary holder	Eppendorf, Hamburg, Germany	Cat #: 920007392
Customized +10D contact lens (3.0 mm diameter, 1.6 mm BC, PMMA clear)	Advanced Vision Technologies, CO, USA	N/A
Diagnosys ERG Celeris	Diagnosys LLL, Littleton, MA, USA	Celeris Model #: D430
Dual-Stage Glass Micropipette Puller	Narishige international USA, NY, USA	Model PC-10
Femtojet® Express Electronic microinjector	Eppendorf, Hamburg, Germany	Cat #: 920010521
Foot control pedal	Eppendorf, Hamburg, Germany	Cat #: 920005098
Heating pad	K&H Manufacturing, CO, USA	Model HM10
Heidelberg OCT Spectralis	Heidelberg Engineering, Germany	N/A
Leica DM4000 B LED automated upright microscope system	Leica Microsystems, San Francisco, CA	N/A
Leica M165 FC fluorescent stereo microscope	Leica Microsystems, San Francisco, CA	N/A
Leica MZ6 modular stereomicroscope	Leica Microsystems, San Francisco, CA	N/A
Micropipette Grinder	Narishige international USA, NY, USA	Model EG-401

(*Continued on next page*)

Continued

REAGENT or RESOURCE	SOURCE	IDENTIFIER
Near-infrared machine	Spectral Instruments Imaging, Tuscon, AZ, USA	Lago X system
Positioning aids	Eppendorf, Hamburg, Germany	Cat #: 920005829
Syringe cleaning wire	Hamilton Company, Reno, NV, USA	Part/REF #: 18300
VWR® micro cover glass	VWR International, LLC, Radnor, PA, USA	Cat. # :48393-081
VWR® Superfrost® Plus Micro Slide	VWR International, LLC, Radnor, PA, USA	Cat. #: 48311-703

RESOURCE AVAILABILITY

Lead contact

Further information and requests for resources should be directed to and will be fulfilled by the lead contact, Vinit B. Mahajan (vinit.mahajan@stanford.edu). All stable reagents generated in this study are available from the lead contact with a completed Materials Transfer Agreement.

Materials availability

This study did not generate new unique reagents.

Data and code availability

- All data generated in this paper will be shared by the lead contact by request.
- This paper does not report original code.
- Any additional information required to reanalyze the data reported in this work paper is available from the lead contact upon request.

EXPERIMENTAL MODEL AND SUBJECT DETAILS

Mice

Specific pathogen-free 6-week-old male and female wild-type BALB/c mice were purchased from Envigo. Specific pathogen-free 6-week-old male and female wild-type C57BL/6J were purchased from the Jackson Laboratory, USA. Mice were maintained in the Animal Care Facilities at the Stanford University. All protocols were approved by the Institutional Animal Care and Use Committees of the Stanford University.

METHOD DETAILS

In vitro release profiling of a model drug implant (Cy5.5/PLGA)

1. Suspend one Cy5.5/PLGA implant in 60 μL of PBS supplemented with bovine serum albumin (BSA/PBS, 0.1%, w/v) to prevent the precipitation of hydrophobic free Cy5.5 during the test, and keep the test tubes at 37°C.
2. At 1-, 2-, 4-, and 7-days, briefly vortex the tubes, spin down, remove 30 μL of supernatant, and replace with 30 μL of fresh BSA/PBS solution. Store the collected supernatant at -20°C before the measurement.
3. After the last collection, dissolve the remaining implants by adding DMSO at an equivalent volume of remaining BSA/PBS (final solvent composition is 1:1 = DMSO:BSA/PBS), vortexing thoroughly, and incubating at room temperature for 10 minutes. The amount of remaining dye in the implants is determined with a standard curve of free dye dissolved in DMSO:BSA/PBS cosolvent.
4. Measure the fluorescent intensity (λex = 650 nm; λem = 714 nm) of the collected supernatants in a 384 flat black well plate to determine the Cy5.5 concentration at each time point.
5. To produce a cumulative release profile, determine the dye amount in nmol released into the buffer at each time point.

Equation : $Cumulative\ amount\ of\ Cy5.5_t = \left([Cy5.5]_t * 0.06\ mL\right) + \left([Cy5.5]_{t-1} * 0.03\ mL\right)$

6. Plot the amount of Cy5.5 dye released (nmol) v. time (days) (Figure S1B). For a cumulative percentage release profile, divide individual values by the total amount of dye determined to be in the intact implant.

$$\textbf{Equation}: \textit{Cumulative \% of dye released from implant} = \frac{\textit{Cumulative amount of Cy5.5}_t}{\textit{Initial amount of Cy5.5 in implant}} * 100$$

Microcapillary tube fabrication

To fabricate a microcapillary tube injection without relying on traditional microfabrication preformed in a clean room, we used a capillary fabrication procedure with a micropipette puller and a borosilicate glass capillary with an inner and outer diameter of 0.58 and 1.00 mm, respectively (Figure S2A) (Wert et al., 2012; Chan et al., 2020; Wang et al., 2014). This procedure allows local stretch at the site of heating (the middle section of the glass capillary) without impacting the cross sections of both glass capillary ends. For ODI injection purposes, an inner diameter of ~50 μm is optimal for the pulled glass capillaries. The following is the step-by-step procedure for microcapillary pulling:

1. Turn the micropipette puller on (Dual-Stage Glass Micropipette Puller; PC-10, Narishige international USA, NY, USA).
2. Set the heating temperature to 67°C (Figure S2A, panel 1).
3. Adjust the pulling-weight applied to the pulling module.

Note: As long as the glass capillary can be partially pulled and meets the inner diameter of 50 μm, the applied pulling-weight can be flexible.

4. Place a borosilicate glass microcapillary (1B100-4, World Precision Instruments, FL, USA) on the pulling clamps.

Note: Position the microcapillary so the desired pulling-part is in the middle of the heating ring.

5. Turn the heater (heating ring) of the micropipette puller on.
6. As the microcapillary heats up, it will be stretched by the weight of the pulling-weight (Figure S2A, panel 1).
7. Cut the narrowest part of the pulled microcapillary by using a clean forceps to make a needle (Figure S2A, panel 2).

Note: Typically, the narrowest part of the microcapillary is located near the bottom end of the heating ring.

8. Adjust the needle length to about 3 to 4 mm using a clean forceps (Figure S2A, panels 4 and 5).

Note: Perform this step using a dissecting microscope.

Needle polishing

For the intravitreal injection, it is necessary to insert the needle into the posterior segment of the eye rather than the anterior segment. This allows the drug to be delivered directly to the retina without dosing the anterior segment. The mouse posterior segment has an average thickness of approximately 180 μm (Horio et al., 2001; Schmucker and Schaeffel, 2004). Its outer layer consists of multiple layers of tissue (i.e., sclera, choroid, retina), and its inner chamber is filled with vitreous humor, a semi-viscous fluid, that helps to maintain the spherical shape of the eye. These anatomical features generate strong enough resistance against trauma during penetration of the injection needle. A sharpened needle is necessary to perform a good intravitreal injection to deliver an implant into the vitreous chamber. To sharpen the injection needle, we ground the tip of the needle using a micropipette grinder. The following is the step-by-step procedure for needle polishing:

1. Turn the micropipette grinder on (EG-401, Narishige international USA, NY, USA; Figure S2A, panel 6).
2. Set the motor speed to 2,000 rpm.
3. Place the length-adjusted needle in the micromanipulator.
4. Load double distilled H_2O to the wheel cleaner syringe.
5. Turn on the valve of the wheel cleaner and soak the whetstone.

Note: This will prevent overheating of the needle and remove ground debris.

6. Set the angle of micromanipulator to 30°.

Note: This makes a 30° slanted needle, which is optimized for sclera penetration.

7. Adjust the x- and y-axis positions of the micromanipulator so the needle touches the whetstone (Figure S2A, panel 6).
8. Stop grinding when the needle opening reaches about 80 to 100 μm (Figure S2A, panel 7).

Note: Final needle tip dimensions are shown in Figure 2B.

9. Sterilize the needle by autoclaving.

Implant loading

The mechanical properties of polymeric implants used for the ODI formulations are sturdy enough to retain their shape and size for microcapillary needle injections (e.g., biodegradable polymers: poly(lactic-co-glycolic acid) (PLGA), polylactic acid (PLA), polyglycolic acid (PGA), and polycaprolactones (PCL); non-biodegradable polymers: ethylene vinyl acetate (EVA), silicone, and polyimide/polyvinyl alcohol (PVA) (Maya-Vetencourt et al., 2020; Shmueli et al., 2013). By considering the size of rodent eyes (~3.2 mm axial length for adult mice; ~4.6 mm axial length for adult rats; Figure 1) and the inner diameter of the needle, the implant dimensions are determined as 0.5 - 2 mm in length and 80 - 100 μm in diameter. The following is the step-by-step procedure for implant loading:

1. Sterilize the tools with 70% ethanol.
2. Under a dissecting microscope, align the implant with the tip of a needle and move the implant into the needle bevel using a fine forceps (Figure S2A, panel 8).
3. Gently load the implant into the needle using the forceps until the implant is fully in the needle (Figure S2A, panel 9).

Note: To prevent damage to the needle, avoid contacting the sharpened needle tip with the forceps.

4. Using a pipette loaded with a gel-loading tip, load 1 μl of PBS into the needle (Figure S2A, panels 10 and 11).

Note: The PBS should fill the needle cavity around the implant.
Note: The PBS is loaded to prevent the introduction of air into the vitreous chamber during the injection.

Rodent handling

The mouse was anaesthetized by ketamine and xylazine based on its body weight (0.08 mg ketamine/g and 0.01 mg xylazine/g) according to the Administrative Panel of Laboratory Animal Care (APLAC) and the Institutional Animal Care and Use Committee (IACUC)-approved protocols at Stanford University. After the mouse was anesthetized, 1% tropicamide ophthalmic solution (Sandoz inc. NJ, USA) was applied to the eyes to dilate the pupils. The whiskers were trimmed, and the coat near the eyes was dampened with PBS so the whiskers and the coat hairs would not obscure the eye and interfere with the injection (Figure S4). Lubricant eyedrops (Alcon, TX, USA) were applied before the injection to prevent corneal dryness.

1. Weigh the animal and calculate the correct dosage of the ketamine and xylazine injection mixture.
2. Using one hand, restrain the mouse with the abdomen facing up.
3. Perform the intraperitoneal injection with the ketamine and xylazine mixture using a 20 G needle.
4. Place the mouse on the heating pad (HM10, K&H Manufacturing, CO, USA).
5. Apply 1% tropicamide to help with the pupil dilution.
6. Trim the whiskers to prevent microscope examination disruption.
7. Wet around the eye with clean 1X PBS.
8. Wait for 5 minutes for the mouse to become anesthetized.
9. Apply lubricant eyedrops (Refresh Tears® Lubricant Eye Drops, Allergan; Cat #: NDC 0023-0798-01) to the eye to prevent the cornea surface from drying out.

Note: Apply one drop per eye every 5 minutes.

Implant injection

Depending on the size, weight, and physical property of an implant, two different injection methods can be performed: injection by air pressure (**M1** below); injection by plunger (**M2** below). We recommend testing injection by air-pressure first because it requires a simpler surgical setup. However, this method, unlike injection by plunger, is limited by the physical properties of the implant.

M1. Implant injection by air-pressure

To inject an implant by air-pressure, an electronic microinjector commonly used for intravitreal injection of fluids was utilized. The following is the step-by-step procedure for the electronic microinjector setup (**M1-a**), the surgery bed setup (**M1-b**), and the surgical process (**M1-c**) for an implant injection by air-pressure:

M1-a. The electronic microinjector setup.

1. Turn on the electronic microinjector (Femtojet Express, Eppendorf; Cat #: 920010521) and run a self-test.
2. Assemble the needle with the capillary holder (Eppendorf, Cat #: 920007392) and positioning aids (Eppendorf, Cat #: 920005829) (Figures S2B and S2C).
3. Connect the injection device to the electronic microinjector.
4. Set up a working parameter for the electronic microinjector: 500 hPa injection pressure, 1.0 second injection time.

S1-b. Surgery bed setup.

1. Set a heating pad on the surgery bed to maintain the body temperature of the mouse (Figure S2D).

Note: The preset of the heating pad used was 37°C.

2. Transfer an anesthetized animal to the surgery bed for surgery.

3. Apply lubricant eyedrops to the eyes to prevent the cornea surface from drying out.

S1-c. Implant injection.

1. Sterilize the needle and capillary holder (Eppendorf, Cat No: 920007392) with 70% ethanol (Figure S2E).
2. Load the needle to a capillary holder attached to a positioning aid.
3. Hold and adjust the animal's head using the non-dominant hand, and perform the injection using the dominant-hand.
4. Gently insert the needle into the eyeball.

Note: The recommended needle entry-position is 2 mm posterior to the limbus.
Note: The needle is perpendicular to the eye surface.
Note: The recommended depth of the needle head is 2 to 3 mm.

5. Hit the foot control pedal (Eppendorf, Cat #: 920005098) to engage the electronic microinjector.
6. Once the implant is delivered, slowly remove the needle from the eyeball.
7. Apply the antibiotic ophthalmic solution to the eye to prevent potential infections.
8. Place the post-surgical mouse on a heating pad until it wakes up.

Note: Throughout the procedure, keep applying one lubricant eyedrop every 5 minutes to prevent the cornea surface from drying out.

M2. Implant injection by plunger

To inject an implant by plunger, a micromanipulator and a syringe-cleaning wire were utilized. The following is the step-by-step procedure to make the plunger (**M2-a**), assemble the injection module (**M6-b**), and set up the micromanipulator and the surgery bed (**M2-c**). The surgical process (**M2-d**) for an implant injection by plunger is also detailed:

M2-a. Implant plunger. To generate an implant plunger, a syringe cleaning wire (18300, Hamilton Company, Reno, NV, USA) was used. To adjust the thickness of the implant plunger to fit into the needle, one end of the syringe cleaning wire was ground using a Black Arkansas stone (Dan's Whetstone Company Inc., Pearcy, AR, USA) until the diameter of the wire was 50 μm. The following is the step-by-step procedure for making the implant plunger:

1. Apply a syringe-cleaning wire on the Black Arkansas stone.
2. Using your pointer finger, press and move one end of the cleaning wire back and forth.
3. After 10 repetitions, check the width under a dissecting microscope.
4. Repeat step 3 until the diameter of the wire reaches 50 μm (Figure S3A).
5. (Optional) By banding the non-ground end of the cleaning wire, make a handle-like structure that can be used to easily manipulate the plunger during surgery.

M2-b. Injection module assembly. An injection module was assembled to mount the implant loaded needle to the micromanipulator (Figure S3B). The following is the step-by-step procedure for injection module assembly:

1. Sterilize the needle and capillary holder with 70% ethanol.
2. Assemble the implant loaded needle to a capillary holder.

Note: This step should be done with care so that the implant does not fall out of the needle.
Note: Parafilm the needle and the capillary holder together to provide a more stable assembly.

3. Insert the plunger into the hole at the opposite end of the needle tip.
4. Keep the plunger at the halfway point of the implant loaded needle.

Note: The plunger should not be touching the implant.

M2-c. Micromanipulator and surgery bed setup. For the intravitreal injection, stability of the microcapillary during the surgery is very important. Since the mouse eye is small and fragile, any unnecessary movement or vibration from the surgical hand may damage or tear the eyeball during injection. There are several commercially available micromanipulators with angle specific adjustable arms. In our MI3 method, utilizing a micromanipulator provides a precise and stable position to fine-tune the needle holder angle. Also, it secures the needle position and supports a smooth injection when using the plunger. The following is the recommended setup for the micromanipulator and the surgical platform for the intravitreal injection of ODIs:

1. Install the micromanipulator right next to the animal surgical platform.
2. Set the angle of the needle holder on the micromanipulator to 30° (Figure S3C).
3. Raise the surgical bed to meet the height limitation of the micromanipulator.
4. Place the heating pad on top of the surgical bed.
5. Set the heat to maintain the body temperature of the mouse.

Note: The preset of the heating pad used was 37°C.

6. Place the implant and plunger loaded needle on the micromanipulator (Figure S3C).
7. Adjust the micromanipulator location, making the needle and eye visible under the dissecting microscope's examination stage (Figure S3D).

M2-d. Implant injection.

1. Using the micromanipulator's x-axis adjustment knob, move the needle closer to the injection site Video S1).
2. Apply lubricant eyedrops to the eye to prevent the eye from drying.
3. Slowly adjust the x-axis adjustment knob until the needle is inserted into the eye.

Note: The recommended needle entry-position is 2 mm posterior to the limbus.

4. Insert the needle until the tip of the needle can be seen in the eye under the dissecting microscope.

Note: The recommended depth of the needle head is 2 to 3 mm.

5. Move the plunger from the bottom of the microcapillary until its end touches the implant.
6. Gently push the implant into the eye.
7. When the implant is fully inserted, slowly remove the needle by adjusting the x-axis adjustment knob.
8. Apply an antibiotic ophthalmic solution to the eye to prevent potential infections.
9. Place the post-surgical mouse on a heating pad until it wakes up.

Infrared-SLO and OCT imaging

After the mice were anesthetized, the pupils were dilated by applying a 1% tropicamide sterile ophthalmic solution (Alcon Laboratories, Fort Worth, TX), and a customized +10D contact lens (3.0 mm diameter, 1.6 mm BC, PMMA clear, Advanced Vision Technologies) was applied to the dilated pupil. The retina fundus images were captured with the Heidelberg Spectralis SLO/OCT system (Heidelberg Engineering, Germany) equipped with an 870 nm infrared wavelength light source and a 30°C lens (Heidelberg Engineering). The OCT scanner has a 7 μm optical axial resolution, a 3.5 μm digital resolution, and a 1.8 mm scan depth at a 40 kHz scan rate. The mouse retina was scanned with the horizontal scan mode centered by the optic nerve head at 100 frames average under high-resolution mode (each B-scan consisted of 1536 A scans).

Eye/retina sectioning, H&E stain, and histology imaging

Mice eyes were enucleated and fixed as previously described (Mahajan et al., 2011). Experimental samples and related control eyeballs were processed in parallel. For hematoxylin and eosin (H&E) staining, enucleated eyeballs were fixed in Excalibur's Alcoholic Z-Fix (Excalibur Pathology, Norman, OK) for 24 hours at room temperature. The eyes were then embedded in paraffin, sectioned at 10 μm, and placed on slides (VWR International, LLC, Radnor, PA). The slides were air-dried and placed in a 60°C oven overnight. The slides were cooled down, deparaffinized by water and stained with Hematoxylin (Mercedes Scientific, Lakewood Ranch, FL) and Eosin (Fisher Scientific, Hampton, NH) showing preservation of all tissue substructures. For the histological imaging, all slides were imaged under an automated upright Microscope (Leica DM4000 B LED), and Leica software was used for image processing.

Electroretinogram

The mice were dark-adapted overnight, and manipulations were conducted under dim light illumination while recordings were made using Espion ERG Diagnosys equipment (Diagnosys LLL, Littleton, MA). The mice were anesthetized by an intraperitoneal injection of 0.1 mg/10 g body weight of anesthesia [0.9 ml ketamine –100 mg/ml (Akorn, Lake Forest, IL) and 0.5 ml xylazine –20 mg/ml (Akorn, Lake Forest, IL) in 8.6 ml PBS]. The pupils were dilated with a 1% tropicamide sterile ophthalmic solution (Alcon Laboratories, Fort Worth, TX). Body temperature was maintained at 37°C using a heating pad during the procedure. Electrodes were placed on the corneas, and refresh lubricant eye gel (Allergan, Irvine, CA) was applied to each eye. Both eyes were recorded simultaneously.

In vivo fluorescence imaging of a model drug implant (Cy5.5/PLGA) in mouse eyes and dye quantification

After 3 days post-injection of the implant and the equivalent amount of free dye (18 ng in 2 μL of BSA/PBS), mouse eyes were enucleated from mice. Non-injected eyes were visualized as controls. The fluorescent signal of Cy5.5 (λex 640 nm / λem 710 nm, exposure: 120 sec) was monitored on a Lago X system (Spectral Instruments Imaging, Tucson, Arizona). For quantification of the remaining dye in the eyes, the enucleated eyes were digested using a tissue digestion buffer (100 mM Tris-HCl (pH 8.0), 100 mM EDTA, 100 mM NaCl, 1% SDS, 20 units/mL proteinase K) at 55°C overnight. Fifty μL of DMSO was added to the digestion solution (final ratio of DMSO:digestion buffer is 1:1) and the mixtures were rocked at room temperature for 30 min to dissolve the hydrophobic implant. Supernatants including free dye were collected by centrifugation at 16,000 x g for 5 min, and the dye concentration was determined by measuring fluorescent intensities (λex 650 nm / λem 714 nm) using a standard curve with free dye dissolved in a DMSO/digestion buffer.

QUANTIFICATION AND STATISTICAL ANALYSIS

In OCT imaging, retinal thickness was measured with Heidelberg Spectralis built in thickness measurement where thickness of each layer was defined as the average thickness in the circular scans centered on optic nerve head (ONH). Four thickness measurements were evaluated: the whole retina thickness, defined as the distance from retinal nerve fiber layer (RNFL) to retinal pigment epithelium (RPE); the ganglion cell complex (GCC), defined as the thickness of RNFL, ganglion cell layer (GCL) and inner plexiform layer (IPL); the

photoreceptor (RP) thickness, defined as distance from outer plexiform layer (OPL) to outer segment (OS); and the RPE thickness. The thickness data were summarized as means and standard error of the means (SEM) for six biological replicates. Paired t-tests were used for comparison of different layer thickness and ERG signals of control eye and PLGA injected eye using GraphPad Prism software.

For quantification of the remaining Cy5.5 model drug in the eyes, the dye concentration in enucleated eyes was determined by measuring fluorescent intensities (λex 650 nm / λem 714 nm) using a standard curve with free dye dissolved in a DMSO/digestion buffer. The amount of Cy5.5 were summarized as means and standard error of the means (SEM) for six biological replicates of implant-injected eye, four biological replicates of free-drug-injected eye, and four biological replicates of control eye. 1-way ANOVA followed by Tukey's multiple comparisons test (****$p<0.0001$) was used for comparison of each group using GraphPad Prism software.